Crack nucleation at stress concentration points in composite materials - application to crack deflection by an interface

Dominique Leguillon, Eric Martin

CRACK NUCLEATION AT STRESS CONCENTRATION POINTS IN COMPOSITE MATERIALS — APPLICATION TO CRACK DEFLECTION BY AN INTERFACE

Dominique Leguillon* and Eric Martin†
*Institut Jean Le Rond d'Alembert CNRS UMR 7190
Université Pierre et Marie Curie, 4 place Jussieu, 75005 PARIS, France
†Laboratoire des Composites Thermo-Structuraux CNRS UMR 5801
Université Bordeaux 1, 3 rue La Boétie, 33600 PESSAC, France

Abstract

The coupled criterion predicts crack nucleation at a stress concentration point. It is a twofold criterion that uses conditions for energy and tensile stress and involves both the toughness and tensile strength of the material. In general, the crack jumps a finite length and then either stops or goes on growing. The criterion has proven its effectiveness in many situations encountered in homogeneous materials like V- and U-notches and predictions agree reasonably with experimental measurements. It can also be used to study specific mechanisms of degradation of composites such as delamination or fibre debonding. It has recently been used successfully to predict the initiation of delamination from a stress-free edge; the application discussed in this chapter is the deflection of transverse cracks by an interface. However, it is valid for both delamination between layers and fibre debonding.

10.1 Introduction

Delamination is the main cause of failure of multimaterials and especially of composite laminates: the components separate leading to total failure or at least to a weakened structure. This topic is still the subject of numerous contemporary works and a detailed and recent list of references can be found in Martin *et al.* [1], which will give a better overview of the problem. There are at least two important origins of delamination under

static load [2]: the first is the classic initiation process, which occurs at the intersection of a free edge with the interface between two layers. It is a zone of stress concentration described in elasticity by a singular displacement field [1, 3]. The other is less obvious because it is an internal process and therefore not directly detectable: the deflection of transverse cracks present in the most disoriented layers relative to the tensile direction [4–6]. The classical situation in a laminate concerns the presence of plies oriented 90° with respect to the loading direction. Transverse microcracks are then generated, which coalesce to form a transverse crack that is deflected when it reaches the interface with a 0° ply. This deflection mechanism creates a delamination crack [7]. Crack deflection at the fibre/matrix interface is also a prerequisite for the activation of toughening mechanisms like multiple matrix cracking in ceramic matrix composites (CMCs) [8, 9].

We propose in this chapter to present the coupled criterion, which predicts crack nucleation at stress concentration points [10]. It combines stress and energy conditions that do not require the definition of a characteristic fracture length selected more or less arbitrarily. This criterion has been applied successfully to several situations in composite materials: delamination originating from a stress-free edge within a generalized plane-strain elasticity framework [1, 11] and crack kinking out of an interface within a plane-strain framework [12, 13]. It is illustrated here by the second mechanism mentioned above, transverse crack deflection by an interface. The analysis will be developed for plane strain and could be theoretically extended to 3D although a number of technical difficulties remain [14].

10.2 The Coupled Criterion

To establish this criterion, a good generic model is the three-point bending test on a V-notched specimen made of a homogeneous material (Fig. 10.1).

In composite materials, the criterion applies at the intersection of the interface between two layers and a free edge for instance [1], or at the end of a transverse crack impinging on an interface as illustrated in the next sections.

The coupled criterion uses two conditions to predict the nucleation of cracks in areas of stress concentrations in brittle materials: the maximum tensile or shear stress that the structure can sustain and an energy balance between the stored energy and the energy required to induce fracture [10].

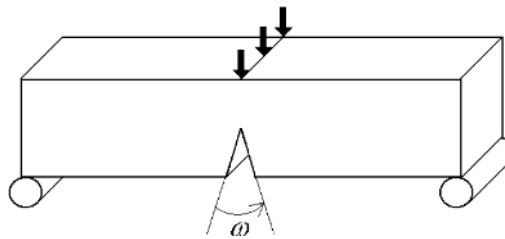

Fig. 10.1. The three-point bending test on a V-notched homogeneous specimen.

The first condition refers to the tensile strength σ_c (or shear strength τ_c) while the other relies on the toughness G_c of the material (or interface). These two conditions must be satisfied simultaneously.

The form taken by these two conditions is from the theory of singularities and the asymptotic expansions of the displacement field $\underline{U}$ and the stress field $\underline{\underline{\sigma}}$ in the vicinity of the origin, the so-called Williams' expansion (in polar coordinates with origin at the singular point formed by the notch root):

$$\begin{cases} \underline{U}(r,\theta) = \underline{R} + kr^{\lambda}\underline{u}(\theta) + \cdots \\ \underline{\underline{\sigma}}(r,\theta) = kr^{\lambda-1}\underline{\underline{s}}(\theta) + \cdots \end{cases} \tag{10.1}$$

λ is the singularity exponent ($1/2 \leq \lambda \leq 1$ for a V-notch), k (MPa·m$^{1-\lambda}$) is the generalized stress intensity factor (GSIF), $\underline{u}(\theta)$ and $\underline{\underline{s}}(\theta)$ are two angular functions and $\underline{R}$ is a constant (the rigid translation of the origin). Coefficient k depends on the whole geometry of the structure and on the remote applied load. The exponent and the angular functions depend only on the local geometry and elastic properties; they are solutions to an eigenvalue problem and are either known analytically in some simple cases or can anyway be determined numerically using a simple algorithm. Clearly the stress components tend to infinity as $r \to 0$; this is why it is called a singular point.

Note that here and in the following, we only address the tensile stress but extension to the shear component is straightforward.

The GSIF k can be computed using a path-independent integral Ψ [15, 16], valid for any elastic fields satisfying the equilibrium to 0 (i.e. vanishing boundary conditions and the balance equation within the domain

surrounded by the integration path):

$$k = \frac{\Psi(\underline{U}(r,\theta), r^{-\lambda}\underline{u}^{-}(\theta))}{\Psi(r^{\lambda}\underline{u}(\theta), r^{-\lambda}\underline{u}^{-}(\theta))} \quad \text{with}$$

$$\Psi(\underline{U},\underline{V}) = \frac{1}{2}\int_{\Gamma} (\underline{\underline{\sigma}}(\underline{U})\cdot\underline{n}\cdot\underline{V} - \underline{\underline{\sigma}}(\underline{V})\cdot\underline{n}\cdot\underline{U})\mathrm{d}s, \tag{10.2}$$

where Γ is a contour encompassing the notch root and starting and finishing on the stress-free edges of the notch and $\underline{n}$ is its normal pointing toward the origin. Relation (10.2) is based on two properties:

(1) If λ is an eigenvalue then so is $-\lambda$. The so-called dual mode [15] or 'super singular' function [17] $r^{-\lambda}\underline{u}^{-}(\theta)$ is a mathematical solution to the previous eigenvalue problem, which has presently no special physical meaning (in particular, the elastic energy associated with this function is unbounded in the vicinity of the origin).

(2) For any pair of eigensolutions $r^{\alpha}\underline{u}_{\alpha}(\theta)$ and $r^{\beta}\underline{u}_{\beta}(\theta)$, $\beta \neq -\alpha \Rightarrow \Psi(r^{\alpha}\underline{u}_{\alpha}(\theta), r^{\beta}\underline{u}_{\alpha}(\theta)) = 0$. This is a kind of bi-orthogonality property (note that Ψ is not a scalar product), which allows extraction of the coefficient k. This result is a consequence of the path independence of Ψ.

Here, the only role of the dual mode is to be a mathematical extraction function; however, these modes will play a greater role in the matched asymptotic procedures both for the inner and outer expansions (see (10.14) and (10.15) in Section 10.3).

The stress condition (e.g. the maximum tensile stress criterion) involves the tensile component σ of the stress tensor $\underline{\underline{\sigma}}$ acting on the presupposed crack path defined by the direction θ_0 prior to its onset; it provides an upper bound to the admissible crack extension lengths a ($\lambda - 1 < 0$):

$$\sigma = kr^{\lambda-1}s(\theta_0) + \cdots \geq \sigma_c \quad \text{for} \quad 0 \leq r \leq a \Rightarrow ka^{\lambda-1}s(\theta_0) \geq \sigma_c. \tag{10.3}$$

The coefficient $s(\theta_0)$ is a dimensionless constant derived from $\underline{\underline{s}}$, which can be normalized to $s(\theta_0) = 1$ if the failure direction (i.e. θ_0) is known [15]. Relation $(10.3)_2$ is enough to imply $\sigma \geq \sigma_c$ along the whole presupposed crack path since σ is a decreasing function of the distance to the singular point.

As will be shown in Section 10.3, expansions (10.1) can be used to define an expansion of the potential energy variation when a small crack

extension appears in direction θ_0. Its leading term provides a lower bound of the crack extension length ($2\lambda - 1 > 0$):

$$G^{\text{inc}}(\theta_0) = -\frac{W(a) - W(0)}{a} = A(\theta_0) k^2 a^{2\lambda-1} + \cdots \geq G_c, \tag{10.4}$$

where $W(x)$ is the potential energy of the structure embedding a crack extension with length x. $G^{\text{inc}}(\theta_0)$ is the so-called incremental energy release rate, because it depends on the increment a; emphasis is put on the fact that we do not consider the limit as $a \to 0$ as for the Griffith criterion [18]. The incremental and differential criterion are identical if $\lambda = 1/2$. $G^{\text{inc}}(\theta_0)$ is the rate of potential energy change prior to and following the onset of a new crack with length a. The scaling coefficient $A(\theta_0)$ (MPa^{-1}) is another constant depending on the local properties and on the direction θ_0 of the short crack but not on the remote applied load which occurs in (10.4) through the only coefficient k. A complete definition of A is given in the following section.

The compatibility between these two inequalities provides a characteristic length a_c at initiation (Fig. 10.2):

$$a_c = \frac{G_c}{A(\theta_0)} \left(\frac{s(\theta_0)}{\sigma_c} \right)^2. \tag{10.5}$$

Initiation is in general (i.e. if $\lambda > 1/2$) an unstable mechanism. The crack jumps the length a_c and then continues to grow or not, but a_c is not defined as a crack arrest length. Essentially, below this length the balance between the stored energy and the energy consumed during failure does not hold: no crack smaller than a_c can be observed. This jump length is still a function of θ_0.

Then we deduce an Irwin-like [19] condition on the GSIF k, which plays the classical role of the stress intensity factor (SIF) K_I

$$k \geq k_c = \left(\frac{G_c}{A(\theta_0)} \right)^{1-\lambda} \left(\frac{\sigma_c}{s(\theta_0)} \right)^{2\lambda-1}. \tag{10.6}$$

For a crack embedded in a homogeneous body, then $\lambda = 1/2$ and $k = K_I$, relation (10.6) coincides with the well-known Irwin criterion. A straight edge in a homogeneous material is a limit case where there is no stress concentration, then $\lambda = 1$ and inequality (10.6) coincides with the maximum tensile stress criterion.

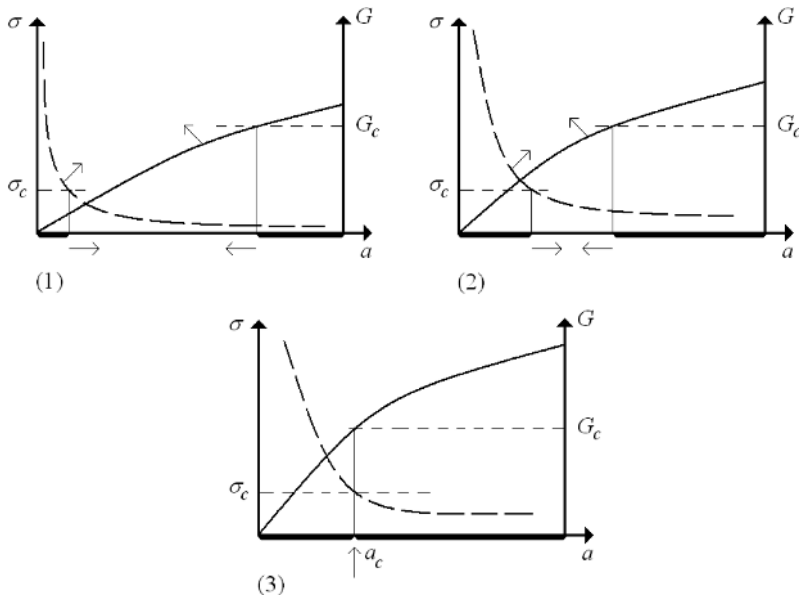

Fig. 10.2. Schematic view of the determination of a_c (10.5). (1) For a small remote load, crack extension lengths fulfilling the stress and the energy conditions are incompatible. (2) When the remote load increases, the two bounds are closer to each other. (3) Failure occurs when the two bounds merge giving a_c. Arrows indicate the motion of the curves and points when the remote load increases.

The direction θ_0 was assumed to be known; if not, one has to check all the possible directions and maximize the denominator in (10.6), i.e. minimize the value of k_c.

A single mode is involved in (10.1); for a V-notch this corresponds to the symmetric case as shown in Fig. 10.1. Generalizations can be made to account for more complex loadings, where it is then necessary to determine both the load causing failure and the direction of the nucleating crack [20].

The computation of the scaling coefficient $A(\theta_0)$, using matched asymptotic expansions, will be the topic of the next section. For simplicity the dependency on θ_0 will be omitted.

Remark: Martin [1, 21, 22] and Hebel [23] and their co-workers apply the coupled criterion numerically without going through the semi-analytical asymptotic expansion procedure. The tensile stress σ along the presupposed crack path and the incremental energy release rate G^{inc} (10.4) are extracted from a direct finite element (FE) computation, which requires taking special

care with the mesh refinement in the vicinity of the region where the new crack initiates. Inequalities (10.3) and (10.4) are employed without calculating λ, k, s and A, and reduce to

$$\sigma = \sigma_{\mathrm{FE}}(r) \geq \sigma_c \quad \text{for} \quad 0 \leq r \leq a \quad \text{and}$$

$$G^{\mathrm{inc}} = -\frac{W_{\mathrm{FE}}(a) - W_{\mathrm{FE}}(0)}{a} \geq G_c. \tag{10.7}$$

a is the smaller length fulfilling the two inequalities. Indeed (10.7) is the most general definition of the coupled criterion and can be used in all cases.

This approach allows situations to studied, which cannot be taken into account in the asymptotic approach, like crack arrest after a short initiation for instance. However, it does not reveal directly (analytically) the role played by the different geometric parameters of the structure, such as the layer thickness for an adhesive layer or an interphase for instance [24].

10.3 Matched Asymptotic Expansions

Numerically solving an elasticity problem in a domain Ω^a embedding a short crack of length a at the root of a V-notch (Fig. 10.3) presents some difficulties because of the small size of the perturbation. Drastic mesh refinements are needed for the very small details.

It is better to represent the solution in the form of an outer expansion or far field:

$$\underline{U}^a(x_1, x_2) = \underline{U}^0(x_1, x_2) + \text{small correction}, \tag{10.8}$$

where $\underline{U}^0$ is the solution to the same elasticity problem but now posed on the unperturbed domain Ω^0 (Fig. 10.1), which can be considered as the limit of Ω^a as $a \to 0$ (the short crack is not visible).

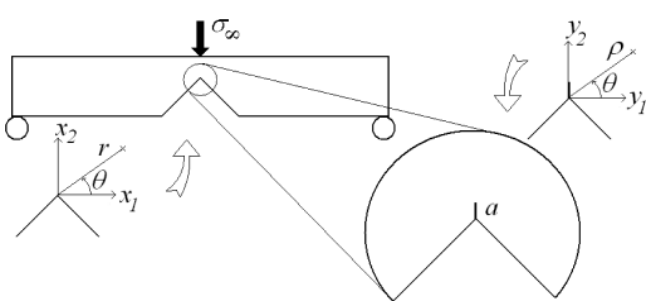

Fig. 10.3. Onset of a short crack of length a at the root of the V-notch.

It is clear that this solution $\underline{U}^0$ is a satisfying approximation of $\underline{U}^a$ away from the perturbation, i.e. outside a neighbourhood of it, hence its designation as the outer field (or far field or remote field).

Evidently, this information is incomplete, particularly when we are interested in fracture mechanisms. We therefore dilate the space variables by introducing the change of variables $y_i = x_i/a$. In the limit when $a \to 0$, we obtain an unbounded domain Ω^{in} (looking like the enlarged frame in Fig. 10.3) in which the length of the crack is now equal to 1.

We then look for a different representation of the solution in the form of an expansion known as the inner expansion or near field:

$$\begin{aligned}\underline{U}^a(x_1, x_2) = \underline{U}^a(ay_1, ay_2) = F_0(a)\underline{V}^0(y_1, y_2) \\ +F_1(a)\underline{V}^1(y_1, y_2) + \cdots,\end{aligned} \tag{10.9}$$

where $F_1(a)/F_0(a) \to 0$ as $a \to 0$. Since there are no conditions at infinity to give well-posed problems for $\underline{V}^0$ and $\underline{V}^1$, matching rules are used. There must be an intermediate zone (close to the perturbation for the far field and far from it for the near field) where both the inner and outer expansions are valid.

The behaviour of the far field near the origin is described by the expansion in powers of r as previously encountered in Eq. (10.1):

$$\underline{U}^0(x_1, x_2) = \underline{R} + kr^\lambda \underline{u}(\theta) + \cdots \tag{10.10}$$

Then the matching conditions can be written as follows:

$$F_0(a)\underline{V}^0(y_1, y_2) \approx \underline{R}, \quad F^1(a)\underline{V}^1(y_1, y_2) \approx ka^\lambda \rho^\lambda \underline{u}(\theta), \tag{10.11}$$

when $\rho = r/a = \sqrt{y_1^2 + y_2^2} \to \infty$ (the symbol $\approx$ means here 'behaves as at infinity'), thus

$$F_0(a) = 1; \quad \underline{V}^0(y_1, y_2) = \underline{R}; \quad F_1(a) = ka^\lambda; \quad \underline{V}^1(y_1, y_2) \approx \rho^\lambda \underline{u}(\theta). \tag{10.12}$$

This matching statement is nothing else than the so-called remote load at infinity. Using superposition, it becomes:

$$\underline{V}^1(y_1, y_2) = \rho^\lambda \underline{u}(\theta) + \hat{\underline{V}}^1(y_1, y_2) \quad \text{with} \quad \hat{\underline{V}}^1(y_1, y_2) \approx 0. \tag{10.13}$$

More precisely, the behaviour of $\underline{\hat{V}}^1(y_1, y_2)$ at infinity can be described by the dual mode $\rho^{-\lambda}\underline{u}^-(\theta)$ to $\rho^{\lambda}\underline{u}(\theta)$ (see Section 10.2):

$$\underline{\hat{V}}^1(y_1, y_2) = \kappa\rho^{-\lambda}\underline{u}^-(\theta) + \cdots \tag{10.14}$$

This expansion is analogous to (10.10) but is at infinity; κ is the GSIF and missing terms tend to 0 faster than $\rho^{-\lambda}$ at infinity. This detail is generally useless for our purpose but it may play a role elsewhere. It has been used recently to determine the length of a crack using full field measurements and digital image correlation (DIC) [25]. It allows the small correction mentioned in (10.8) to be specified:

$$\underline{U}^a(x_1, x_2) = \underline{U}^0(x_1, x_2) + k\kappa a^{2\lambda}(r^{-\lambda}\underline{u}^-(\theta) + \underline{\hat{U}}^1(x_1, x_2)) + \cdots \tag{10.15}$$

Finally Eq. (10.9) becomes

$$\underline{U}^a(x_1, x_2) = \underline{U}^a(ay_1, ay_2) = \underline{R} + ka^{\lambda}\underline{V}^1(y_1, y_2) + \cdots \tag{10.16}$$

The function $\underline{V}^1(y_1, y_2)$ is computed using FEs in an artificially bounded (at a large distance from the perturbation) domain with either prescribed displacements or forces along the new fictitious boundary.

We have now at our disposal a description of the elastic solution prior to and following the onset of a short crack and we are able to calculate the change in potential energy $W(a) - W(0)$, which can be expressed using the path independent integral Ψ encountered in (10.2)

$$-(W(a) - W(0)) = \Psi(\underline{U}^a, \underline{U}^0). \tag{10.17}$$

Then, substituting the above expansions, once for $a = 0$ and once for $a \neq 0$, into (10.17) leads to the expression (10.4) with $G^{\text{inc}} = -(W(a) - W(0))/a$ and

$$A = \Psi(\underline{V}^1(y_1, y_2), \rho^{\lambda}\underline{u}(\theta)). \tag{10.18}$$

Figure 10.4 shows the dimensionless function $A^* = E^*A$ (where $E^* = E$ for plane stress and $E^* = E/(1-\nu^2)$ for plane strain, with E being Young's modulus and ν Poisson's ratio for the homogeneous isotropic material) for different V-notch openings ω (Fig. 10.1) and for a crack located along the bisector (symmetric case). It can be used as a master curve valid for any elastic isotropic material; the role of Poisson's ratio in A has been verified numerically. Note that $A^* = 2\pi$ for $\omega = 0^\circ$ as a consequence of the normalization of the eigenmode (10.1). The tensile stress $\sigma = k/r^{\lambda-1}$ along

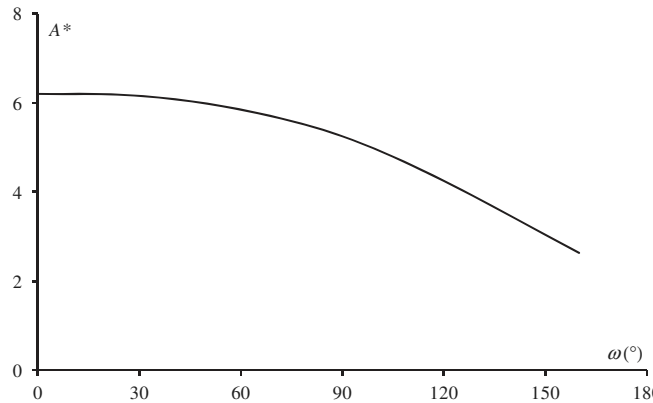

Fig. 10.4. The dimensionless coefficient A* vs. the V-notch opening ω in the symmetric case.

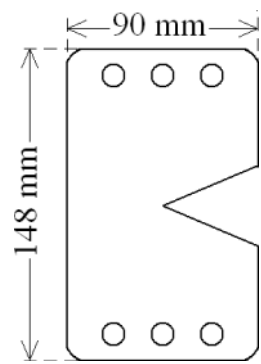

Fig. 10.5. PMMA Compact Tension V-notched Specimen (CTS).

the bisector, leading to $\sigma = k/\sqrt{r}$ for $\omega = 0°$ (a crack) whereas it is usually $\sigma = k/\sqrt{2\pi r}$.

10.4 Application to the Crack Onset at a V-Notch in a Homogeneous Material

Tensile tests have been carried out on poly(methyl methacrylate) (PMMA) V-notched specimens ($E = 3250\,\text{MPa}$, $\nu = 0.3$, $\text{G}_\text{c} = 0.325\,\text{MPa.mm}$, $\sigma_\text{c} = 75\,\text{MPa}$) for different V-notch openings from 30 to 160° (Fig. 10.5) [26].

The tensile test was then numerically simulated by finite elements for an arbitrary prescribed load F_0 (note here that special care must be taken given

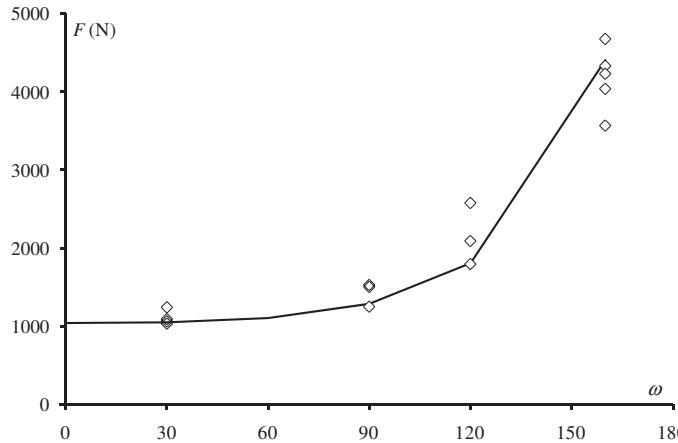

Fig. 10.6. Applied force F at failure of V-notched specimens of PMMA as a function of the notch opening ω. Comparison between experiments (diamonds) and prediction (solid line) using the coupled criterion [26].

Fig. 10.7. Schematic view of a transverse crack impinging on an interface.

the lack of symmetry of the specimen) and the GSIF k_0 was extracted using (10.2). A scaling with the critical value k_c (10.6) provides the corresponding force $F = F_0 \times k_c/k_0$ at failure. A comparison between predicted and measured failure forces is illustrated in Fig. 10.6, which exhibits a fair agreement.

10.5 Application to the Deflection of Transverse Cracks

We now consider a transverse crack as depicted schematically in Fig. 10.7. Despite there being a pre-existing crack, the singular exponent at its tip, which impinges the interface, is not 1/2 as usual and the situation differs from that of a crack in a homogeneous material (Fig. 10.8). For

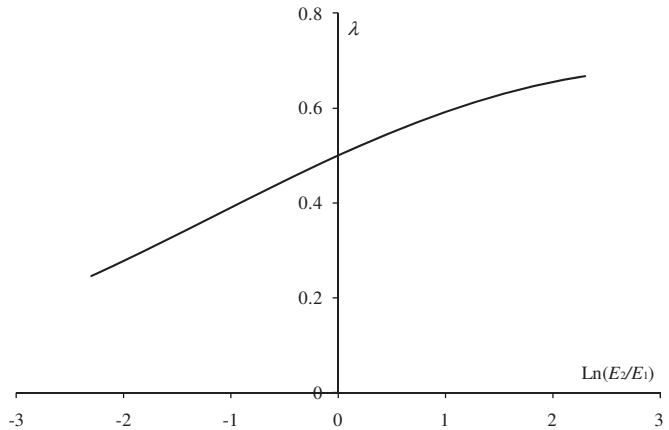

Fig. 10.8. Singular exponent vs. ratio of Young's moduli for two adjacent materials with the same Poisson's ratio $\nu_1 = \nu_2 = 0.3$.

homogeneous isotropic components, if $E_2 > E_1$ (the first case) then $\lambda > 1/2$ (a weak singularity, which is less harmful than a crack) and *vice versa* if $E_2 < E_1$ (the second case) then $\lambda < 1/2$ (a strong singularity, more harmful than a crack). Here E_i is Young's modulus for ply number i (it is assumed that the two Poisson's ratios ν_1 and ν_2 are equal, otherwise the rule is close to the above but slightly altered by the contrast in ν). This obviously leads to substantially different results in terms of rupture. We immediately notice according to (10.4) that if $a \to 0$ then $G^{\text{inc}} \to 0$ in the first case whereas $G^{\text{inc}} \to \infty$ in the second.

This property also affects the (differential) energy release rate G of a crack approaching and crossing the interface. As the crack approaches the interface, there remains a ligament of length l between the crack tip and the interface (Fig. 10.13) and $G \to 0$ (respectively, $G \to \infty$) for a weak singularity (respectively, strong singularity) as $l \to 0$. Symmetrically, after crossing the interface the crack tip is at a distance a from it (Fig. 10.7) and G increases from 0 (weak singularity) or decreases from infinity (strong singularity) as a increases. This behaviour is shown in Fig. 10.9 for different ratios of Young's moduli: $E_2/E_1 = 0.1$, 0.2, 0.5, 1, 2, 5 and 10. The results were obtained using FEs and a variable crack tip location, counted negative if the crack is growing toward the interface and positive after the crossing (Fig. 10.9). Even if the energy is globally calculated at the structure level, it requires strong mesh refinement in the area of interest to give a good geometrical description.

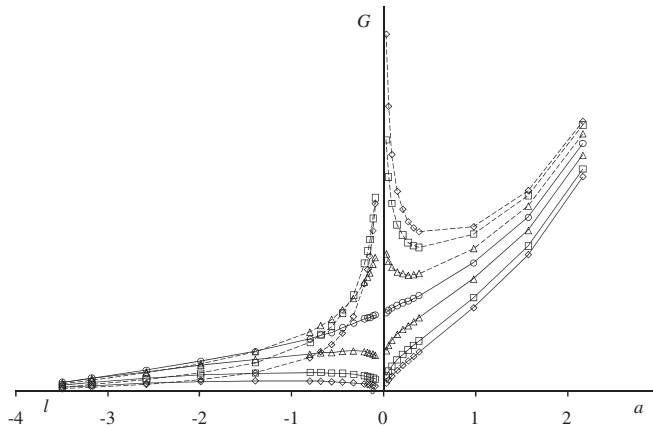

Fig. 10.9. The behaviour of the energy release rate when a crack approaches an interface (left) and then crosses it (right) for different ratios of Young's moduli: $E_2/E_1 = 0.1$ (dashed line and diamonds), 0.2 (dashed line and squares), 0.5 (dashed line and triangles), 1 (solid line and circles), 2 (solid line and triangles), 5 (solid line and squares) and 10 (solid line and diamonds). The units are not important, the emphasis is on the general trends — whether they are increasing or decreasing functions when approaching the interface.

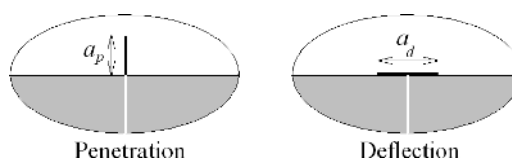

Fig. 10.10. The mechanisms of crack penetration and deflection.

The question that arises now is: does such a transverse crack stop, penetrate Material 2 or deflect along the interface to give a delamination crack (Fig. 10.10)?

Let us consider again inequality (10.4) for two cases: penetration of Material 2 (index p) and deflection along the interface (index d). $G_c^{(I)}$ and $G_c^{(2)}$ are the interface and Material 2 toughness, respectively:

$$G_d^{\text{inc}} = A_d k^2 a_d^{2\lambda-1} + \cdots \geq G_c^{(I)} \quad \text{and} \quad G_p^{\text{inc}} = A_p k^2 a_p^{2\lambda-1} + \cdots \geq G_c^{(2)}. \tag{10.19}$$

Two cases can be considered: a doubly symmetric deflection (Fig. 10.10) or a single asymmetric one; the only change is in the coefficient A_d but this

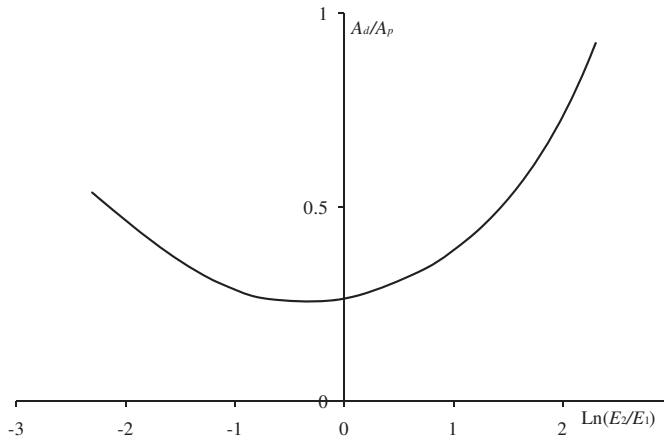

Fig. 10.11. Dimensionless ratio A_d/A_p vs. ratio of Young's moduli for two adjacent materials for a doubly symmetric deflection.

does not lead to a big difference [27]. The following analysis will be carried out for the first case.

Deflection is promoted if the first inequality in (10.19) is fulfilled whereas the second one is not, then:

$$\frac{G_c^{(I)}}{G_c^{(2)}} = R \leq \frac{A_d}{A_p}\left(\frac{a_d}{a_p}\right)^{2\lambda-1}. \tag{10.20}$$

The dimensionless ratio A_d/A_p is plotted in Fig. 10.11 for various values of E_2/E_1 (E_i is the Young's modulus of material i and $\nu_1 = \nu_2 = 0.3$).

He and Hutchinson [28] obtained a similar result (although differently) but simplified thanks to a dubious assumption. They considered the (differential) energy release rates G_p and G_d respectively at the tip of a penetrated crack and a deflected one, the two crack extensions being equal, i.e. $a_d = a_p$, and obtained a condition for the toughness ratio of the interface and Material 2, which is clearly equivalent to the ratio A_d/A_p according to (10.19) if $a_d = a_p$:

$$R \leq \frac{G_d}{G_p}. \tag{10.21}$$

A discussion of this specific point can be found in [29, 30].

Clearly it is possible to determine the two characteristic lengths a_d and a_p in (10.20) using the stress condition, provided $\lambda > 1/2$ (otherwise both

G and σ are decreasing functions of the distance to the singular point and the coupled criterion can no longer be used).

10.5.1 $\lambda > 1/2$

If $\lambda > 1/2$, according to (10.5) ($\sigma_c^{(I)}$ and $\sigma_c^{(2)}$ are the tensile strengths of the interface and Material 2, respectively):

$$a_d = \frac{G_c^{(I)}}{A_d}\left(\frac{s_d}{\sigma_c^{(I)}}\right)^2 ; \quad a_p = \frac{G_c^{(2)}}{A_p}\left(\frac{s_p}{\sigma_c^{(2)}}\right)^2 . \tag{10.22}$$

Thus deflection is promoted if

$$R \leq \frac{A_d}{A_p}\left(\frac{s_d}{s_p}\frac{\sigma_c^{(2)}}{\sigma_c^{(I)}}\right)^{\frac{2\lambda-1}{1-\lambda}} . \tag{10.23}$$

The special case $\lambda = 1$ cannot be met; it would correspond to an infinitely compliant Material 1 compared to Material 2. Knowing that the ratio s_d/s_p remains of the same order of magnitude as 1, it is clear from (10.23) that the tensile strength ratio plays a crucial role, which can significantly alter the criterion proposed by He and Hutchinson.

As illustrated in Fig. 10.12, deflection will be favoured even more as Material 2 becomes increasingly resistant (i.e. $\sigma_c^{(2)} > \sigma_c^{(I)}$). Note that

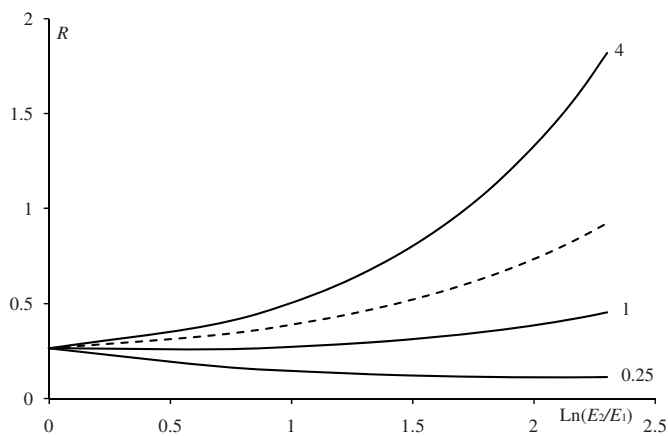

Fig. 10.12. Failure map of the criterion (10.23) for different values of the ratio of strengths $\sigma_c^{(2)}/\sigma_c^{(I)} = 0.25$, 1, 4 as a function of the material contrast E_2/E_1. The dashed line corresponds to A_d/A_p (Fig. 10.11). Below the continuous line conditions are favourable for deflection along the interface, and above to penetration of Material 2.

Parmigiani and Thouless [31] derived the same tendency with cohesive zone models (CZMs).

Reference is made in both cases to the tensile stress; this is clear for penetration but less obvious for deflection. However, considering the eigenmode governing the stress field before crack propagation, one can check that the tensile component σ is equal to or larger than the shear one τ: the ratio σ/τ grows from 1 to 2.8 as E_2/E_1 varies from 1 to 10. In addition, knowing that shear failure is generally more difficult than tension, it seems reasonable to consider only the tensile component.

This analysis could be included in a homogenization process where the domain shown in Fig. 10.7 would be a representative volume element (RVE). The slenderness of this cell can be used to take into account the different densities of transverse cracks [5].

10.5.2 $\lambda < 1/2$

If $\lambda < 1/2$ then this coupled criterion approach is not valid because the energy release rate is now a decreasing function of the distance to the singular point (see (10.4)) and the energy condition no longer gives any lower bound for the crack extension length [27, 32]. Under a monotonic loading the crack grows continuously: there is no crack jump. Moreover, according to (10.19), G_d and G_p tend to infinity as a_d and a_p decrease to 0, which prevents the direct use of the energy release rate at the very start of the crack growth process. No rigorous conclusion can be derived in this situation. He and Hutchinson [28] still proposed to use (10.21) or equivalently the ratio A_d/A_p. Another approach based on the maximum dissipated energy is proposed in Leguillon *et al.* [27]; however, this corresponds better to the geometrical situation analysed in the next section (Fig. 10.13).

10.6 The Cook and Gordon Mechanism

Due to the decay to 0 or the unbounded growth of the energy release rate (Fig. 10.9), it should be pointed out that the geometric situation shown in Fig. 10.7 cannot be achieved by a crack growing in Material 1 and approaching the interface. It can only be obtained by a mechanical action like a saw cut.

Otherwise, we have to consider a crack in Material 1 with its tip a small distance l from the interface as shown in Fig. 10.13 [32, 33].

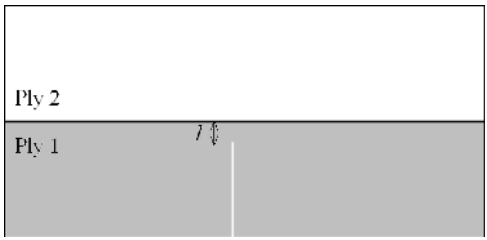

Fig. 10.13. A crack growing in Material 1 and approaching the interface, at a distance l.

Assuming a small increment $\delta l \ll l$ at the tip of this crack and according to (10.4), the (differential) energy release rate is

$$G_1 = -\lim_{\delta l \to 0} \frac{W(l+\delta l) - W(l)}{\delta l} = k^2 A_1 \lim_{\delta l \to 0} \frac{(l+\delta l)^{2\lambda} - l^{2\lambda}}{\delta l} + \cdots$$
$$= 2\lambda k^2 A_1 l^{2\lambda - 1} + \cdots \tag{10.24}$$

A_1 is given by (10.18) where the perturbation is the small ligament with width l instead of a crack extension. Moreover, since the crack is growing in Material 1:

$$G_1 = G_c^{(1)} \Rightarrow k^2 l^{2\lambda-1} = \frac{G_c^{(1)}}{2\lambda A_1}. \tag{10.25}$$

This relation means that in these conditions knowing l or the applied load is somewhat equivalent.

10.6.1 $\lambda > 1/2$

If $\lambda > 1/2$, G_1 decreases to 0 as $l \to 0$ and thus drops below $G_c^{(1)}$ (Material 1's toughness). An overload must occur for the situation to evolve. There is a three-way conflict: the crack still grows in Material 1, the interface debonds ahead of the crack tip or the crack jumps and penetrates Material 2 (Fig. 10.14) [34]. The latter mechanism will not be discussed here. Another mechanism called step-over, where the crack reinitiates in the second material, leaving a ligament in its wake, was discussed in [22, 32, 35].

There are now two small parameters l and a_d (respectively, a_p) for debonding (respectively, penetration), which is an additional difficulty. If one is very small compared to the other, it can be neglected in a first step. If they are of the same order of magnitude the expansions can be carried out with either of them. For technical reasons it is easier to use l.

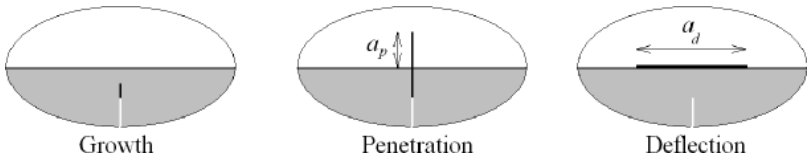

Fig. 10.14. The conflict between the crack growing in Material 1, the crack jumping in Material 2 and the interface debonding.

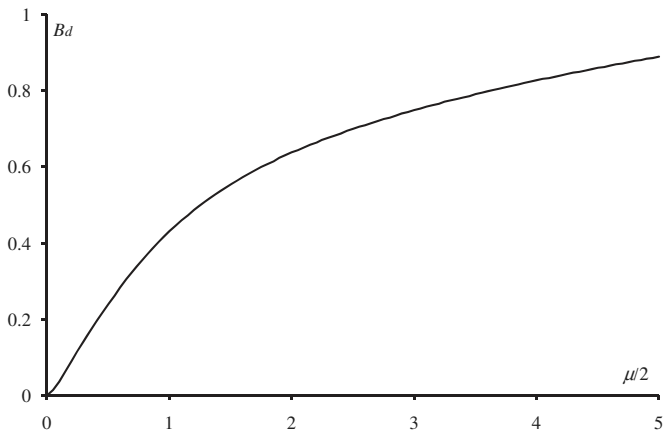

Fig. 10.15. $B_d(\mu)$ (MPa^{-1}) for material contrast $E_2/E_1 = 10$.

By analogy with the single parameter case, the stress and energy conditions are now (see [36] for details of the proof):

$$\begin{cases} \sigma = kl^{\lambda-1}\tilde{\sigma}(\mu_d) \geq \sigma_c^{(I)} \\ G_d^{\text{inc}} = k^2 B_d(\mu_d) l^{2\lambda-1} \geq G_c^{(I)}, \end{cases} \tag{10.26}$$

where $\mu_d = a_d/l$. The function B_d (Fig. 10.15) is an increasing function of μ and replaces A_d. It is derived from the calculation of A (10.18). There are four cases: the 'unperturbed' one (Fig. 10.7) and the successive cases illustrated in Fig. 10.13 and the middle and right of Fig. 14. $\tilde{\sigma}$ is a decreasing function (Fig. 10.16), which replaces s and is the tensile stress associated with $\underline{V}^1$ along the presupposed crack path prior to any crack extension (i.e., with the inner term calculated for the geometry of Fig. 10.13).

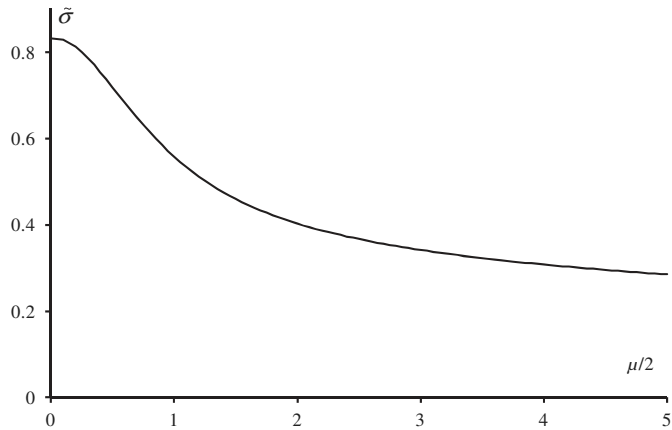

Fig. 10.16. $\tilde{\sigma}(\mu)$ for material contrast $E_2/E_1 = 10$.

The equation for the dimensionless characteristic length μ_d is derived from (10.25) and $(10.26)_2$:

$$B_d(\mu_d) = 2\lambda A_1 \frac{G_c^{(I)}}{G_c^{(1)}}. \tag{10.27}$$

The dimensionless debonding length μ_d is small if the interface toughness $G_c^{(I)}$ is small.

For material contrast $E_2/E_1 = 10$, $\lambda = 0.667$ (Fig. 10.8), $A_1 = 0.479\,\mathrm{MPa}^{-1}$, thus if $G_c^{(I)} = G_c^{(1)}$, then from (10.25) $B_d(\mu_d) = 0.639\,\mathrm{MPa}^{-1}$, $\mu_d/2 = 1.9$ (Fig. 10.15) and $\tilde{\sigma}(\mu_d) = 0.345$ (Fig. 10.16). Thus the condition for an interface debonding ahead of the primary crack is

$$k \geq k_c = \left(\frac{G_c^{(I)}}{B_d(\mu_d)}\right)^{1-\lambda} \left(\frac{\sigma_c^{(I)}}{\tilde{\sigma}(\mu_d)}\right)^{2\lambda-1}. \tag{10.28}$$

Note that (10.25) and $(10.26)_1$ give l, which is not useful for criterion (10.28) which requires only μ_d:

$$l = \frac{G_c^{(1)}}{2\lambda A_1} \left(\frac{\tilde{\sigma}(\mu_d)}{\sigma_c^{(I)}}\right)^2. \tag{10.29}$$

The ligament width is small if the tensile strength $\sigma_c^{(I)}$ is high. Since $a_d = \mu_d l$ and according to (10.27) and (10.29) the debond length is large for a high toughness and a small tensile strength of the interface, which is often the case for polymer adhesives for instance.

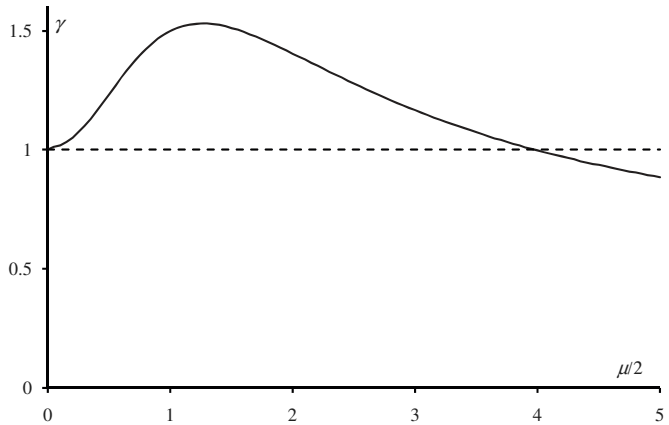

Fig. 10.17. The evolution of the energy release rate (normalized by $G_c^{(1)}$) at the tip of the primary crack after the onset of interface debonding for material contrast $E_2/E_1 = 10$.

The primary crack may stop at a distance l: it depends on how the energy release rate G_1 evolves after the onset of the debonding. Figure 10.17 shows the ratio $\gamma = G_1/G_c^{(1)}$ as a function of the dimensionless debonding length μ_d for $E_2/E_1 = 10$ and with $\nu = 0.3$ in both materials.

Obviously, on the one hand, if the characteristic debonding length μ_d is smaller than a given value (roughly $\mu_d/2 = 4$ in the present case, Fig. 10.17) the energy release rate increases as debonding occurs and the primary crack restarts and definitely breaks the ligament. On the other hand, this ligament does not disappear and can only be observed if the debonding length is large ($\mu_d/2 = 4$ in the present case).

10.6.2 $\lambda < 1/2$

If $\lambda < 1/2$, G_1 increases as $l \to 0$. For a given l, if the load (i.e. a given GSIF k) is such that (10.25) holds then the crack accelerates toward the interface. As it impinges on the interface, there is an excess of energy in the balance:

$$\Delta W_1 = kA_1 l^{2\lambda} - G_c^{(1)} l = G_c^{(1)} \left(\frac{1}{2\lambda} - 1 \right) l. \tag{10.30}$$

Hence, the crack will deflect and the (differential) energy release rate G_d will decrease as the debond length increases (which is calculated using a small increment $\delta a_d \ll a_d$ at the tip of the deflected crack and passing to the limit $\delta a_d \to 0$ as for G_1, see (10.24)). Following (10.24) and (10.25), it

drops below the interface toughness at a distance a_d such that

$$G_d = 2\lambda k^2 A_d a_d^{2\lambda-1} = G_c^{(I)} \Rightarrow \left(\frac{a_d}{l}\right)^{2\lambda-1} = \frac{G_c^{(I)}}{G_c^{(1)}} \frac{A_1}{A_d}. \tag{10.31}$$

At this point, the excess energy is now

$$\Delta W = \Delta W_1 + \Delta W_d = \left(G_c^{(1)} l + G_c^{(I)} a_d\right) \left(\frac{1}{2\lambda} - 1\right). \tag{10.32}$$

Thus the crack will continue to grow with a characteristic length δa_d until it consumes this excess energy:

$$\delta a_d = \frac{\Delta W}{G_c^{(I)}} = \left(\frac{G_c^{(1)}}{G_c^{(I)}} l + a_d\right) \left(\frac{1}{2\lambda} - 1\right). \tag{10.33}$$

Of course $a_d + \delta a_d$ is an upper bound of the delamination length. Some of the excess energy will be dissipated by dynamic effects, such as elastic waves producing noise for example.

As already mentioned, comparison with a crack advancing in a straight line and penetrating Material 2 is not considered here. This mechanism is more difficult to describe and is the subject of a work in progress.

The modelling described in Sections 10.5 and 10.6 can be extended to the anisotropic case provided it can still be split into plane and antiplane problems. This is the case for cross-ply laminates of carbon-fibre-reinforced polymers, where each layer is orthotropic in the appropriate basis, but not for angle-ply laminates [1].

10.7 Conclusion

Plane-strain elasticity is the main framework of this chapter. The coupled criterion can be extended without major difficulty to a generalized plane-strain assumption in the analysis of delamination of angle-ply laminates [1, 11]. It is also possible to describe in the same way crack kinking out of an interface [12, 13], although this makes use of complex exponents and SIFs [37, 38]. Together with the analysis of crack deflection by the interface developed here, this covers a wide range of problems of failure in composite laminates; especially since anisotropy, which has not been mentioned in this chapter, does not complicate things too much as long as the assumption of plane or generalized plane elasticity still holds.

Obviously the extension to 3D raises the most difficulties. There are no major conceptual changes, but everything becomes technically much

more complicated. The crack extension is no longer simply described by two parameters, e.g. direction and length: the complete geometry must be taken into account. An attempt was made to predict the nucleation of small lens-shaped cracks along a straight crack front subject to Mode III remote loading [14]. Nevertheless it is clear that much remains to be done in this domain.

References

[1] Martin E., Leguillon D., Carrere N., 2010. A twofold strength and toughness criterion for the onset of free-edge shear delamination in angle-ply laminates, *Int. J. Solids Struct.*, 47, 1297–1305.

[2] Sridharan S., 2008. Delamination behaviour of composites, in *Materials*, Woodhead Publishing Ltd, Cambridge, UK.

[3] Brewer J.C., Lagace P.A., 1998. Quadratic stress criterion for initiation of delamination, *J. Comp. Mat.*, 122, 1141–1155.

[4] Nairn J.A., Hu S., 1992. The initiation and growth of delaminations induced by matrix microcracks in laminated composites, *Int. J. Fracture*, 57, 1–24.

[5] Delisée I., 1996. Etude de mécanismes de délaminage des composites croisés carbone/epoxy, PhD thesis, Université Pierre et Marie Curie, Paris.

[6] Ladeveze P., Lubineau G., Marsal D., 2006. Towards a bridge between the micro- and mesomechanics of delamination for laminated composites, *Comp. Sci. and Technology*, 66, 698–712.

[7] Blázquez A., Mantič V., París F., McCartney L.N., 2008. Stress state characterization of delamination cracks in [0/90] symmetric laminates by BEM, *Int. J. Solids Struct.*, 45, 1632–1662.

[8] Martin E., Peters P.W.M., Leguillon D., Quenisset J.M., 1998. Conditions for crack deflection at an interface in ceramic matrix composites, *Mat. Sci. Eng. A*, 250, 291–302.

[9] Carrère N., Martin E., Lamon J., 2000. The influence of the interphase and associated interfaces on the deflection of matrix cracks in ceramic matrix composites, *Comp. Part A*, 31, 1179–1190.

[10] Leguillon D., 2002. Strength or toughness? A criterion for crack onset at a notch, *Eur. J. Mech. — A–Solid*, 21, 61–72.

[11] Pipes B.R., Pagano N.J., 1970. Interlaminar stresses in composite laminates under uniform axial extension, *J. Comp. Mat.*, 4, 538–548.

[12] Leguillon D., Murer S., 2008. Crack deflection in a biaxial stress state, *Int. J. Fracture*, 150, 75–90.

[13] Leguillon D., Murer S., 2008. A criterion for crack kinking out of an interface, *Key Eng. Mat.*, 385–387, 9–12.

[14] Leguillon D., 2003. Computation of 3D singular elastic fields for the prediction of failure at corners, *Key Eng. Mat.*, 251–252, 147–152.

[15] Leguillon D., Sanchez-Palencia E., 1987. *Computation of Singular Solutions in Elliptic Problems and Elasticity*, John Wiley & Son, New York, and Masson, Paris.

[16] Labossiere P.E.W., Dunn M.L., 1999. Stress intensities at interface corners in anisotropic bimaterials, *Eng. Fract. Mech.*, 62, 555–575.

[17] Henninger C., Roux S., Hild F., 2010. Enriched kinematic fields of cracked structures, *Int. J. Solids Struct.*, 47, 3305–3316.

[18] Griffith A.A., 1920. The phenomenon of rupture and flow in solids, *Phil. Trans. Roy. Soc. London A*, 221, 163–198.

[19] Irwin G., 1958. Fracture, in *Hand. der Physic*, Springer, Berlin, Vol. VI, pp. 551–590.

[20] Yosibash Z., Priel E., Leguillon D., 2006. A failure criterion for brittle elastic materials under mixed-mode loading, *Int. J. Fracture*, 141, 289–310.

[21] Martin E., Leguillon D., 2004. Energetic conditions for interfacial failure in the vicinity of a matrix crack in brittle matrix composites, *Int. J. Solids Struct.*, 41, 6937–6948.

[22] Martin E., Poitou B., Leguillon D., Gatt J.M., 2008. Competition between deflection and penetration at an interface in the vicinity of a main crack, *Int. J. Fracture*, 151, 247–268.

[23] Hebel J., Dieringer R., Becker W., 2010. Modelling brittle crack formation at geometrical and material discontinuities using a finite fracture mechanics approach, *Eng. Fract. Mech.*, 77, 3558–3572.

[24] Leguillon D., Laurencin J., Dupeux M., 2003. Failure of an epoxy joint between two steel plates, *Eur. J. Mech. A–Solid.*, 22, 509–524.

[25] Leguillon D., 2011. Determination of the length of a short crack at a V-notch from a full filed measurement. *Int. J. Solids Struct.* 48, 884–892.

[26] Leguillon D., Murer S., N. Recho J. Li, 2009. Crack initiation at a V-notch under complex loadings — Statistical scattering, International Conference on Fracture, ICF12, Ottawa, Canada, 12–17 July 2009.

[27] Leguillon D., Lacroix C., Martin E., 2000. Matrix crack deflection at an interface between a stiff matrix and a soft inclusion, *C. R. Acad. Sci. Paris*, 328, série IIb, 9–24.

[28] He M.Y., Hutchinson J.W., 1989. Crack deflection at an interface between dissimilar elastic materials, *Int. J. Solids Struct.*, 25, 1053–1067.

[29] Martinez D., Gupta V., 1994. Energy criterion for crack deflection at an interface between two orthotropic media, *J. Mech. Phys. Solids*, 42, 1247–1271.

[30] He M.Y., Evans A.G., Hutchinson J.W., 1994. Crack deflection at an interface between dissimilar elastic materials: Role of residual stresses, *Int. J. Solids Struct.*, 31, 3443–3455.

[31] Parmigiani J.P., Thouless M.D., 2006. The roles of toughness and cohesive strength on crack deflection at interfaces, *J. Mech. Phys. Solids*, 54, 266–287.

[32] Leguillon D., Lacroix C., Martin E., 2000. Interface debonding ahead of a primary crack, *J. Mech. Phys. Solids*, 48, 2137–2161.

[33] Martin E., Leguillon D., Lacroix C., 2002. An energy criterion for the initiation of interface failure ahead of a matrix crack in brittle matrix composites, *Compos. Interf.*, 9, 143–156.

[34] Cook J., Gordon J.E., 1964. A mechanism for the control of crack propagation in all brittle systems, *Proc. Roy. Soc A*, 282, 508–520.

[35] Quesada D., Picard D., Putot C., Leguillon D., 2009. The role of the interbed thickness on the step-over fracture under overburden pressure, *Int. J. Rock Mech. Min.*, 46, 281–288.

[36] Leguillon D., Quesada D., Putot C., Martin E., 2007. Size effects for crack initiation at blunt notches or cavities, *Eng. Fract. Mech.*, 74, 2420–2436.

[37] Rice J.R., 1988. Elastic fracture mechanics concept for interfacial cracks, *J. Appl. Mech.*, 55, 98–103.

[38] He M.Y., Hutchinson J.W., 1989. Kinking of a crack out of an interface, *J. Appl. Mech.*, 56, 270–278.